CrossMark

An Improved Pair Method to Probe the Dust Extinction Law

Yuxi Wang[1,2,3] , Jian Gao[1,3] , Yi Ren[2,3] , and Jun Li[3]

[1] Institute for Frontiers in Astronomy and Astrophysics, Beijing Normal University, Beijing 102206, China; jiangao@bnu.edu.cn
[2] College of Physics and Electronic Engineering, Qilu Normal University, Jinan 250200, China; yiren@qlnu.edu.cn
[3] Department of Astronomy, Beijing Normal University, Beijing 100875, China

Abstract

Dust extinction law is crucial to recover the intrinsic energy distribution of celestial objects and infer the characteristics of interstellar dust. Based on the traditional pair method, an improved pair method is proposed to model the dust extinguished spectral energy distribution (SED) of an individual star. Instead of the mathematically parameterizing extinction curves, the extinction curves in this work are directly from the silicate-graphite dust model, so that the dust extinction law can be obtained and the dust properties can be analyzed simultaneously. The ATLAS9 stellar model atmosphere is adopted for the intrinsic SEDs in this work, while the silicate-graphite dust model with a dust size distribution of $dn/da \sim a^{-\alpha} \exp(-a/a_c)$, $0.005 < a < 5$ μm for each component is adopted for the model extinction curves. One typical extinction tracer in the dense region (V410 Anon9) and one in the diffuse region (Cyg OB2 #12) of the Milky Way are chosen to test the reliability and the practicability of the improved pair method in different stellar environments. The results are consistent with their interstellar environments and are in agreement with the previous observations and studies, which prove that the improved pair method is effective and applicable in different stellar environments. In addition to the reliable extinction results, the derived parameters in the dust model can be used to analyze the dust properties, which cannot be achieved by other methods with the mathematical extinction models. With the improved pair method, the stellar parameters can also be inferred and the extinction law beyond the wavelengths of observed data can be predicted based on the dust model as well.

Key words: stars: individual (V410 Anon 9, Cyg OB2 #12) – interstellar medium (ISM) – ISM: dust, extinction

1. Introduction

The wavelength dependence of interstellar extinction, which is known as the extinction law or extinction curve, is one of the primary sources of information about the interstellar grain population (Draine 2003). Extinction curves from the ultraviolet (UV) to near-infrared (NIR) bands in the Milky Way (MW) can be characterized by the total-to-selective extinction ratio R_V [$R_V \equiv A_V/E(B-V)$] (Cardelli et al. 1989, hereafter CCM). The value of R_V depends on the interstellar environment along the sight line. The large value of R_V corresponds to the region with high density. For instance, denser clouds tend to have larger values of R_V (≈ 5.5) and the typical diffuse interstellar medium usually has a smaller one ($R_V \approx 3.1$).

The mathematical model is a widely used way to determine the extinction law. In addition to the CCM model, the Fitzpatrick & Massa (1990, hereafter F90) model contains six parameters and can be used to model the shape of extinction curves in UV bands (see Equation (2) in FM90). Fitzpatrick (1999, hereafter F99) estimated new R_V-dependent extinction curves in the MW from UV to IR based on the relationship between R_V and the parameters in the FM90 model, and the F99 model has been updated as the Fitzpatrick (2004, hereafter F04) model.

Although the parameterized extinction models are effective ways to derive the extinction law, they are derived by mathematical parameter fitting rather than based on the physical model. In addition, the mathematical extinction models are not universal in all galaxies, and one model can be only applied to one or some specific galaxies. For example, the MW-type extinction law does not generally apply to the interstellar dust in other galaxies (Clayton et al. 2015), and the single parameter R_V cannot be used to completely describe the extinction feature in the extinction curves in external galaxies (Wang et al. 2022a). Instead, the dust model with the physical basis is another method to obtain the extinction curves. As an extinction curve derived from the dust model presented, the properties of dust can also be obtained, which cannot be analyzed directly from the parameterized extinction curves.

The traditional "pair method" (Bless & Savage 1970), which compares the spectrum of a reddened star with that of an unreddened one with the same or similar spectral type, is universally adopted to determine the dust extinction law in star-resolved galaxies. In this work, the silicate-graphite dust model is adopted to propose an improved pair method, so that the dust extinction law can be obtained and dust properties can be analyzed simultaneously. One extinction tracer located in the dense region of the MW and one located in the diffuse region

of the MW are adopted to test the practicability and the reliability of the improved method. The details of the method are described in Section 2, and the extinction tracers are introduced in Section 3. Section 4 shows our results and discussions. We finally summarize our method in Section 5.

2. Method

Based on the traditional pair method mentioned above, we propose an improved pair method that models the spectral energy distributions (SEDs) in combination with the intrinsic SEDs obtained from the stellar model atmosphere extinguished by the model extinction curves derived from the dust model. With the model SEDs fitting to the observed data, the dust extinction law can be derived, the dust properties can be further analyzed based on the derived parameters in the dust model, and even the stellar parameters can be inferred from the stellar model atmosphere.

Figure 1 summarizes the improved pair method proposed in this work, and the following subsections show the details.

2.1. The Intrinsic SEDs from the ATLAS9 Stellar Model Atmosphere

The traditional pair method considers the spectrum of an unreddened star with the same spectral type as the intrinsic spectrum. However, sometimes it is not easy to obtain the intrinsic spectra from real stars especially in external galaxies because of the limited sample of unreddened standard stars. The stellar model atmosphere can also be used to obtain the standard spectrum, which is at least as accurate as those from the real stars (Fitzpatrick & Massa 2005).

We adopt the ATLAS9 stellar model atmosphere to obtain the intrinsic SEDs in this work. The code is written by Kurucz (1970) and is used for computing the local thermodynamic equilibrium blanketed stellar atmosphere model. The ATLAS9 grid considers effective temperature T_{eff} from 3500 to 50,000 K, surface gravity $\log(g)$ from 0.0 to 5.0 and several chemical compositions.

2.2. The Model Extinction Curves from the Dust Model

As mentioned in Section 1, the extinction curves derived from the dust model are applied in this work. Along the sight line, the extinction at the wavelength of λ can be expressed as:

$$A_\lambda / N_{\mathrm{H}} = 1.086 \int_{a_{\min}}^{a_{\max}} C_{\mathrm{ext}}(a, \lambda) \frac{1}{n_{\mathrm{H}}} \frac{dn}{da} da, \qquad (1)$$

where a is the radius of the dust grain, $C_{\mathrm{ext}}(a, \lambda)$ is the extinction section and can be calculated by Mie theory (Draine & Lee 1984), n_{H} is the number density of H nuclei, N_{H} is the column density of H nuclei, and dn/da is the dust size distribution.

In terms of dust composition, there are mainly the silicate-graphite [+ polycyclic aromatic hydrocarbons (PAH)] model,

the COMP model (silicate, graphite, PAH, amorphous carbon particles, organic refractory material, water ice and voids, Zubko et al. 2004), the silicate core-carbonaceous mantle model (Greenberg 1978; Li & Greenberg 1997) and the composite dust model (Mathis & Whiffen 1989). Three kinds of dust distributions are widely adopted for the silicate-graphite dust model: the power-law size distribution ($dn/da \sim a^{-\alpha}$) proposed by Mathis, Rumpl, and Nordsieck (hereafter MRN, Mathis et al. 1977), the exponentially cutoff power-law size distribution [$dn/da \sim a^{-\alpha} \exp(a/a_c)$] proposed by Kim, Martin and Hendry (hereafter KMH, Kim et al. 1994), and the two log-normal size distributions for two population of PAHs (Li & Draine 2001) adding to the traditional silicate-graphite dust model (Weingartner & Draine 2001).

In this work, we adopt the typical silicate-graphite dust model[4] that consists of spherical amorphous silicate and graphite (Draine & Lee 1984) and choose the KMH dust size distribution for both components: $dn/da \sim a^{-\alpha} \exp(a/a_c)$ in the size range of $0.005 < a < 5 \ \mu\mathrm{m}$, where a is the spherical radius of the dust, α is the power index, and a_c is the exponential cutoff size.

2.3. Compare Model SEDs with the Observed Data

The observed SED F_λ^{obs} of a reddened star can be expressed as (Fitzpatrick & Massa 2005):

$$F_\lambda^{\mathrm{obs}} = F_\lambda^{\mathrm{int}} \theta_R^2 10^{-0.4 A_\lambda}, \qquad (2)$$

where F_λ^{int} is the intrinsic surface flux of the star at wavelength λ, $\theta_R \equiv (R/d)^2$ is the angular radius of the star (where d is the distance and R is the stellar radius), and A_λ is the absolute attenuation of the stellar flux by intervening dust at λ. With the combination of the intrinsic SEDs and the model extinction curves obtained in the previous two subsections, a grid of model SEDs [$F_\lambda^{\mathrm{mod}}(T_{\mathrm{eff}}, \log g, Z, \alpha_{\mathrm{sil}}, a_{c\mathrm{sil}}, \alpha_{\mathrm{gra}}, a_{c\mathrm{gra}})$] can be constructed, where T_{eff}, $\log g$, and Z are, respectively, the effective temperature, the surface gravity, and the metallicity of the extinction tracer, while α_{sil} (α_{gra}) and $a_{c\mathrm{sil}}$ ($a_{c\mathrm{gra}}$) are the power index and the exponential cutoff size in the dust size distribution [$dn/da \sim a^{-\alpha} \exp(a/a_c)$] of silicate (graphite).

Since the model SEDs for the tracers are pre-constructed before the calculation, it is only necessary to compare the observed data with the model SEDs in the template library to

---

4 According to Draine (2011), a class of models that has met with some success assumes the dust to consist of two materials: amorphous silicate and carbonaceous materials. Mathis et al. (1977) showed that models using silicate and graphite spheres could reproduce the observed extinction from the near-IR to the UV. Draine & Lee (1984) presented self-consistent dielectric functions for graphite and silicate and showed that the silicate-graphite model appeared to be consistent with what was known about dust opacities in the far-IR. In addition, the silicate-graphite dust model has been widely used in modeling the dust extinction laws (e.g., MW: Kim et al. 1994; Wang et al. 2015; Magellanic Clouds: Gordon et al. 2003; SN 2014J: Gao et al. 2015; SN 2012cu: Gao et al. 2020; M31: Wang et al. 2022a; M33: Wang et al. 2022b; SN 2010jl: Li et al. 2022) and is the basis of some famous works related to interstellar dust (e.g., Weingartner & Draine 2001; Zubko et al. 2004, etc.).
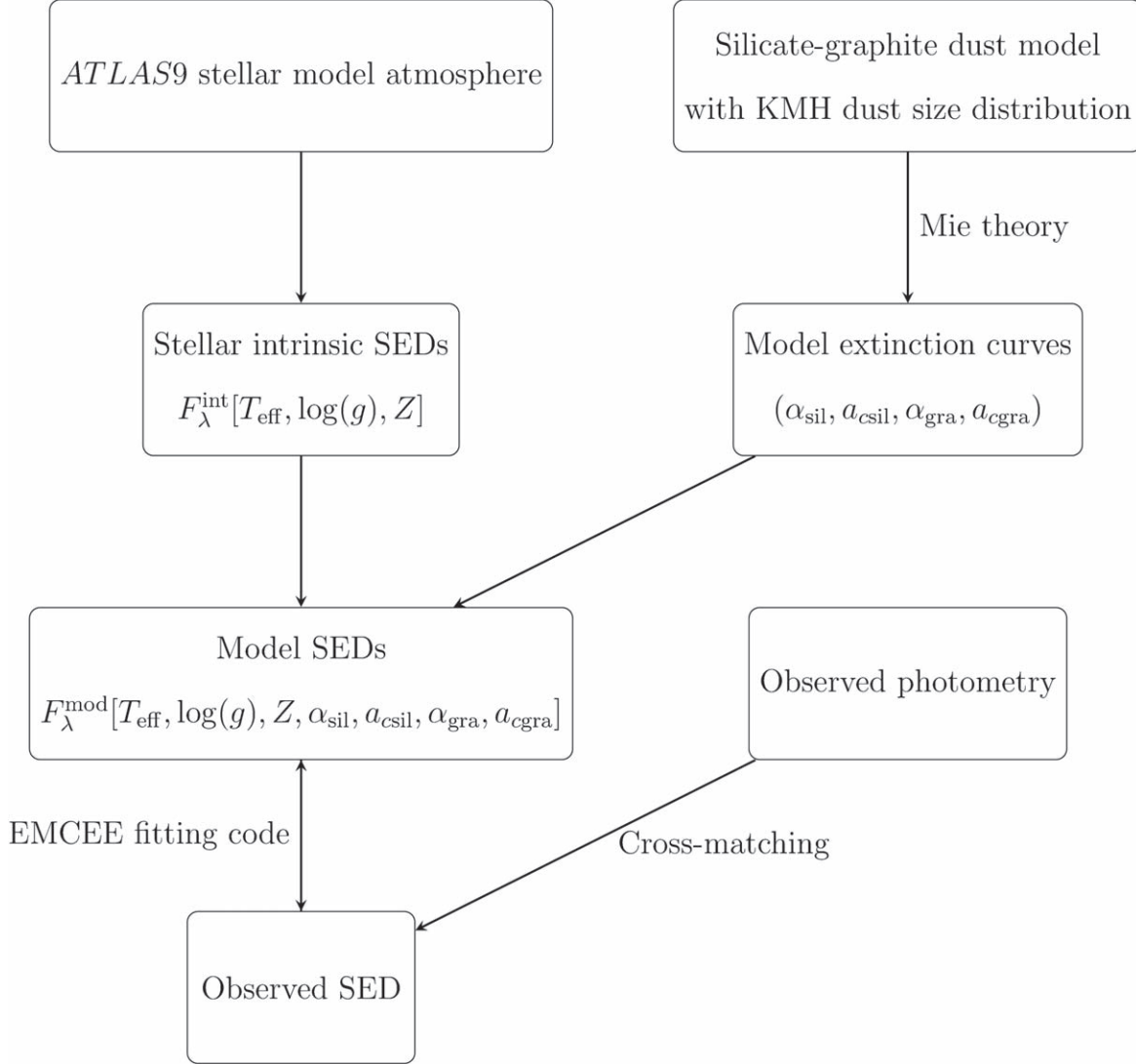
Figure 1. The improved pair method. The intrinsic SEDs from the ATLAS9 stellar model atmosphere and the model extinction curves from the dust model are introduced in Sections 2.1 and 2.2, respectively. The construction of model SEDs and the method that fits the model SEDs to the observed data are presented in Section 2.3.

obtain the dust extinction law. In the application of the method proposed in this work, some prior knowledge (e.g., the stellar parameters, the spectral type of the extinction tracer, etc.) will constrain the range of the parameters and reduce the number of the model SEDs used for comparison, which simplifies the calculation, while the composition of the parameters can be adjusted to balance the complexity of the model and the quality of the fitting.

The EMCEE fitting code (Foreman-Mackey et al. 2013) is adopted in this work to fit the model SEDs to the observed data. It is a Markov Chain Monte Carlo (Goodman & Weare 2010) ensemble sampler based on the Bayesian probability theory (Cox 1946) and helps with the most suitable parameters and the corresponding confidence intervals. We apply the Gaussian likelihood and impose a flat prior on the fitting parameters for the extinction tracers.

We also use the Levenberg–Marquardt method (Weingartner & Draine 2001; Amanullah et al. 2015; Nozawa 2016) for a comparison:

$$\chi^2/\text{d.o.f.} = \frac{1}{N_{\text{data}} - N_{\text{para}}} \sum \frac{(\log(f_{\text{model}}) - \log(f_{\text{observed}}))^2}{\sigma^2},$$
(3)

where N_{data} is the number of the observed photometric points, N_{para} is the number of adjustable parameters, f_{observed} is the

observed flux of each photometric point, f_{model} is the model flux of each photometric point, and σ is the difference between the logarithm of extreme and logarithm of $f_{observed}$. The model SED that fits the observed data best can be found by minimizing the $\chi^2/d.o.f.$, and the corresponding model extinction curve can be regarded as the extinction law and the dust property can be obtained simultaneously.

3. The Extinction Tracers

3.1. The Extinction Tracer in the Dense Region

The main-sequence star named V410 Anon9 is chosen as the extinction tracer in the dense region of the MW. It is located in the vicinity of an actively star-forming cloud (L1495E) within the Taurus-Auriga cloud complex (Strom & Strom 1994). Its spectral type is A2 and the extinction in the V band is $A_V \approx 10$ mag (Strom & Strom 1994; Shenoy et al. 2008), while other members in this cloud are nearly all later than M3 spectral type and their magnitudes of extinction in the V band are much lower. The relatively high brightness and reddening of V410 Anon9 make it a typical extinction tracer for the dense region.

3.1.1. The Observed SED

In this work, we combine the spectroscopic data and the photometric data to construct the observed SEDs of V410 Anon9, which is shown in the upper panel of Figure 2. The spectra are from the Sloan Digital Sky Survey (SDSS, Aguado et al. 2019) and the Large Sky Area Multi-Object Fiber Spectroscopic Telescope (LAMOST, Cui et al. 2012; Zhao et al. 2012). The photometric data, which are listed in Table 1, are from Panoramic Survey Telescope And Rapid Response System (Pan-STARRS, Chambers et al. 2016) in g, r, i, z, y bands, the Two Micron All Sky Survey (2MASS, Cutri et al. 2003) in J, H, K_S bands, the Spitzer/Galactic Legacy Infrared Midplane Survey Extraordinaire (Spitzer/GLIMPSE, Churchwell et al. 2009) in [3.6], [4.5], [5.8], [8.0] bands, the Wide-field Infrared Survey Explore (Cutri et al. 2013) in W_1, W_2, W_3. W_4 bands and GAIA DR2 (Gaia Collaboration 2018) in G_{BP}, G, G_{RP} bands.

However, the original spectra from the LAMOST are uncalibrated. In addition, the extinction curves in the bands covered by the LAMOST spectra and the SDSS spectra (optical bands) do not show the special features as the absorptions in the UV and the IR bands, and the observations in the optical bands cannot restrict the shape of the extinction curves and the dust properties as strongly as those in the UV and IR bands. As a result, only photometric data are adopted to calculate the extinction law. It should be noted that because of the lack of uncertainties in Spitzer/GLIMPSE bands and the quite wide wavelength range of GAIA DR2 G band,[5] we cannot apply these photometric data to determine the extinction curves.
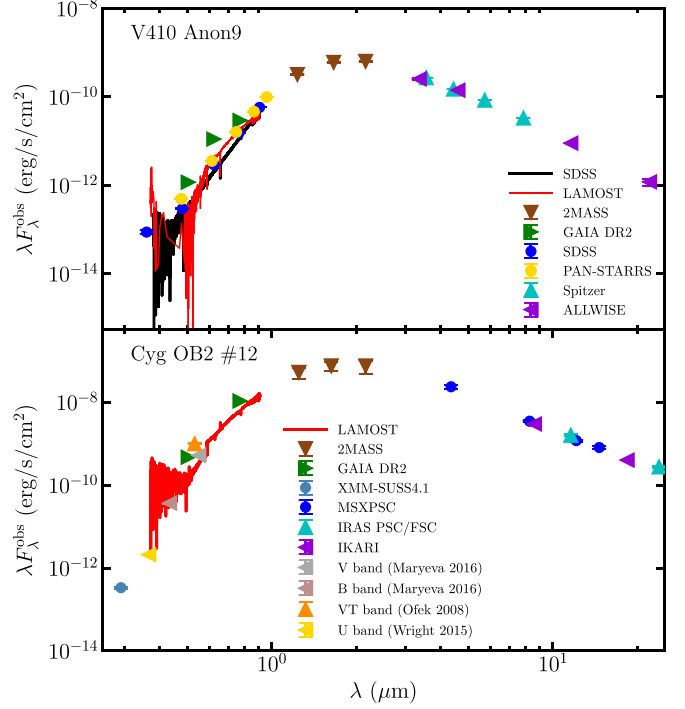

Figure 2. The observed SEDs of V410 Anon9 and Cyg OB2 #12. We only adopt the observed photometry to derive the extinction laws.

3.1.2. The Model SEDs

For the main sequence tracer V410 Anon9, we construct the model intrinsic SEDs with 47 values of the effective temperature ($4000 \leqslant T_{eff} \leqslant 50,000$ K with 1000 K steps), 17 values of surface gravity ($1.00 \leqslant \log(g) \leqslant 5.00$ dex with 0.25 dex steps) and the solar abundances. The intrinsic SEDs from the ATLAS9 stellar model atmosphere are plotted in the upper panel of Figure 3 with gray solid lines. The black dotted line in the upper panel of Figure 3 is the intrinsic SED with the effective temperature set to 8995 K (Strom & Strom 1994) and the surface gravity set to log $(g) = 4.2$ based on the spectral type.[6]

D'Orazi et al. (2011) indicated a solar metallicity for the nearest large star-forming region Taurus-Auriga association where the tracer V410 Anon9 is located. As a result, we adopt the protosolar abundances (Asplund et al. 2009) and assume a typical value of $f_{cs} = 0.3$ for the mass ratio of graphite to silicate, which means that all the Si are constrained in silicate dust and the fraction of gas-phase carbon is 50%. With 56 values of α ($0.5 \leqslant \alpha \leqslant 6.0$ with 0.1 dex steps) and 30 values of a_c ($0.01 \leqslant a_c \leqslant 0.30$ with 0.01 dex steps) considered, a grid of model extinction curves with the same KMH dust distribution for silicate and graphite is constructed for V410 Anon9 after

---

[5] There will be large uncertainty in determining the effective wavelength of the G band because of the wide wavelength range.

[6] V410 Anon9 is an A2 type main-sequence star, of which the surface gravity log(g) is supposed to be under 4.2878 (the typical value for an A5 type main-sequence star, Cox 2000) and over 4.1378 (A0, Cox 2000). We choose the value of 4.2 to represent the surface gravity of V410 Anon9.

Table 1
The Observed Photometry of V410 Anon9 and Cyg OB2 #12

Band	λ_{eff} (μm)	V410 Anon9 Magnitude (mag)	Uncertainty (mag)	Cyg OB2 #12 Magnitude (mag)	Uncertainty (mag)	References
u	0.359	21.389	0.093	…	…	(1)
g	0.481	19.710	0.014	…	…	(1)
r	0.623	16.937	0.004	…	…	(1)
i	0.764	14.945	0.004	…	…	(1)
z	0.906	13.269	0.004	…	…	(1)
g	0.477	19.161	0.028	…	…	(2)
r	0.613	16.744	0.007	…	…	(2)
i	0.748	14.893	0.002	…	…	(2)
z	0.865	13.584	0.006	…	…	(2)
y	0.960	12.648	0.010	…	…	(2)
J	1.235	10.205	0.026	4.667	0.324	(3)
H	1.630	8.717	0.020	3.512	0.260	(3)
K_S	2.160	7.908	0.024	2.704	0.364	(3)
[3.6]	3.550	7.330	…	…	…	(4)
[4.5]	4.439	7.260	…	…	…	(4)
[5.8]	5.731	7.140	…	…	…	(4)
[8.0]	7.872	7.140	…	…	…	(4)
W1	3.350	7.580	0.031	…	…	(5)
W2	4.600	7.235	0.019	…	…	(5)
W3	11.600	7.303	0.020	…	…	(5)
W4	22.100	7.435	0.186	…	…	(5)
G	0.623	15.384	0.001	8.889	0.003	(6)
G_{BP}	0.505	18.127	0.010	11.619	0.006	(6)
G_{RP}	0.772	13.850	0.005	7.441	0.005	(6)
UVW1	0.291	…	…	20.121	0.073	(7)
U	0.365	…	…	17.180	0.034	(8)
B	0.433	…	…	14.760	0.026	(9)
V	0.550	…	…	11.500	0.017	(9)
D	14.650	…	…	1.660	0.069	(10)
C	12.130	…	…	1.847	0.071	(10)
A	8.280	…	…	1.905	0.045	(10)
B2	4.350	…	…	1.885	0.155	(10)
IRAS12	11.600	…	…	2.101	0.037	(11)
IRAS25	12.900	…	…	1.649	0.055	(11)
S9W	8.610	…	…	1.942	0.018	(12)
L18W	18.400	…	…	1.678	0.009	(12)
VT	0.532	…	…	18.810	0.010	(13)

References. (1) Aguado et al. (2019), (2) Chambers et al. (2016), (3) Cutri et al. (2003), (4) Churchwell et al. (2009), (5) Cutri et al. (2013), (6) Gaia Collaboration (2018), (7) Page et al. (2019), (8) Wright et al. (2015), (9) Maryeva et al. (2016), (10) Egan et al. (2003), (11) Abrahamyan et al. (2015), (12) Ishihara et al. (2010), (13) Ofek (2008).

several pre-experiments[7] for reducing the number of the parameters and simplifying the calculation.

With the combination of the intrinsic SEDs and model extinction curves, the model SEDs for V410 Anon9 can be written as $F_\lambda^{\text{mod}}(\alpha_{\text{sil}}, a_{c\text{sil}}, \log T_{\text{eff}}, \log g)$ (or $F_\lambda^{\text{mod}}(\alpha_{\text{gra}}, a_{c\text{gra}}, \log T_{\text{eff}}, \log g)$ for the same dust size distribution).

---

[7] It is found that similar results could be derived from the dust models with the same dust size distribution and the independent dust size distribution.

3.2. The Extinction Tracer in the Diffuse Region

To explore how the improved pair method is applied to different interstellar environments, we choose a typical extinction tracer in the diffuse region for comparison. Located in the stellar association Cygnus OB2, Cygnus OB2 #12 is a Galactic B3-5 hypergiant (Clark et al. 2012; Chentsov et al. 2013). The extinction law toward Cyg OB2 #12 described by standard grain models derived from the former study (Wright et al. 2015) shows consistency to the mean diffuse-ISM curve. Because of its fairly high brightness ($1.9 \times 10^{19} L_\odot$, Clark et al. 2012), it can be used as a popular extinction tracer in the
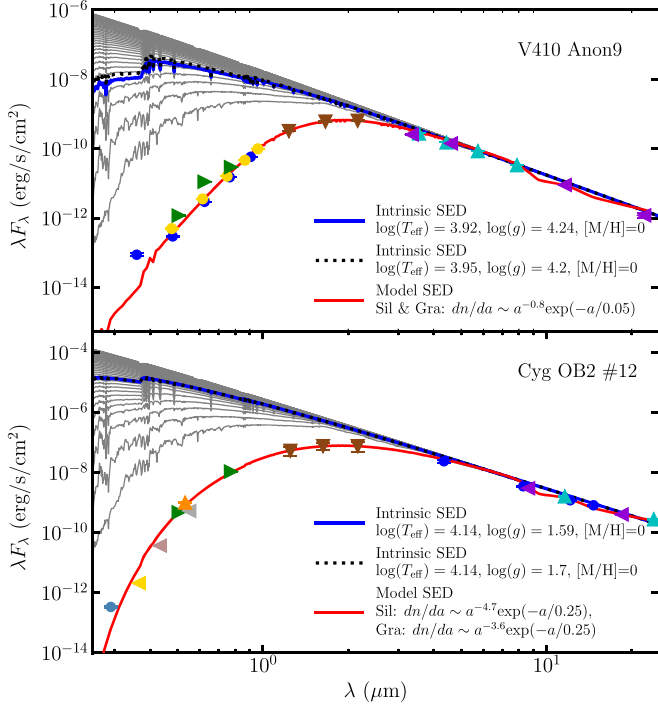
Figure 3. The intrinsic SEDs (gray, black and blue lines) derived from the ATLAS9 stellar model atmosphere for V410 Anon9 and Cyg OB2 #12 as well as the best-fitting SEDs compared with the observed photometry (red solid line). The gray solid lines in the upper panel are the intrinsic SEDs from the ATLAS9 stellar model atmosphere with different effective temperature values and surface gravity values, while the blue solid line is the intrinsic SED with the derived stellar parameters (see Section 4.3 for details).

diffuse region. Many researches on extinction law toward Cyg OB2 #12 have been carried out and indicate that its reddening is higher ($A_V \approx 10.1$ mag, Sharpless 1957; Kiminki et al. 2007; Wright et al. 2015; Hensley & Draine 2020) than the average reddening of bright stars in the association (Hanson 2003; Kiminki et al. 2007; Wright et al. 2010, 2015; Guarcello et al. 2012). Although recent studies suggest that Cyg OB2 #12 may be the member of a binary (Caballero-Nieves et al. 2014; Maryeva et al. 2016; Oskinova et al. 2017) and the system may even consist of a third member (Maryeva et al. 2016), we do not deeply explore its properties as the member in a binary star system in this work and ignore the influence of its possible companion(s).

3.2.1. The Observed SED

The observed SEDs for Cyg OB2 #12 are presented in the lower panel of Figure 2. The spectrum is from the LAMOST (Cui et al. 2012; Zhao et al. 2012). The photometric data used in this work are from GAIA DR2 (Gaia Collaboration 2018) in G_{BP}, G, G_{RP} bands, the 2MASS (Cutri et al. 2003) in J, H, K_S bands, the XMM-Newton Serendipitous Ultraviolet Source

Survey 4.1 (XMM-SUSS 4.1, Page et al. 2019) in $UVW1$ bands, the MSX6C Infrared Point Source Catalog (Egan et al. 2003) in D, C, A, B_2 bands, the InfraRed Astronomical Satellite Point Source Catalog/Faint Source Catalog (IRAS PSC/FSC, Abrahamyan et al. 2015) in IRAS12, IRAS25 bands, the AKARI (Ishihara et al. 2010) in $S9W$, $L18W$ bands, and in U (Wright et al. 2015), B (Maryeva et al. 2016), V (Maryeva et al. 2016), and VT (Ofek 2008) bands.

The observed photometric points for Cyg OB2 #12 are listed in Table 1 and are applied to calculate the extinction law.

3.2.2. The Model SEDs

For Cyg OB2 #12, we also construct the model intrinsic SEDs with 47 values of the effective temperature ($4000 \leqslant T_{\rm eff} \leqslant 50{,}000$ K with 1000 K steps), 17 values of surface gravity ($1.00 \leqslant \log(g) \leqslant 5.00$ dex with 0.25 dex steps) and the solar abundances as mentioned in Section 3.1.2. The intrinsic SEDs from the ATLAS9 stellar model atmosphere are plotted in the lower panel of Figure 3 with gray solid lines. The black dotted line in the lower panel of Figure 3 is the intrinsic SED with the stellar parameters [$T_{\rm eff} = 13700^{+800}_{-500}$ K, log $(g) = 1.70^{+0.08}_{-0.15}$] estimated by Clark et al. (2012).

Whittet (2015) showed that the extinction in the line of sight over the accessible wavelength range is well described by standard grain models that fit the mean diffuse-ISM curve. The element abundances of the diffuse region in the MW are consequently adopted: Si/H ≈ 32 ppm, C/H ≈ 300 ppm, and it is assumed that the mean molecular weight of silicate is 170 per Si (Kim et al. 1994). We derive that the mass ratio of graphite to silicate is $f_{\rm cs} = m_{\rm gra}/m_{\rm sil} = (300 \times 12)/(32 \times 170) \approx 2/3$. $a_{\rm csil}$ and $a_{\rm cgra}$ in the KMH model are fixed to 0.25 μm as mentioned in Wang et al. (2022a), which is the maximum cutoff value of dust size in the MRN model (Mathis et al. 1977). A grid of model extinction curves for Cyg OB2 #12 is thus constructed with 56 values of $\alpha_{\rm sil}$ ($0.5 \leqslant \alpha_{\rm sil} \leqslant 6.0$ with 0.1 dex steps) and 56 values of $\alpha_{\rm gra}$ ($0.5 \leqslant \alpha_{\rm gra} \leqslant 6.0$ with 0.1 dex steps) after the pre-experiments.[8]

With the intrinsic SED extinguished by the model extinction curves, a grid of model SEDs [$F^{\rm mod}_\lambda(\alpha_{\rm sil}, \alpha_{\rm gra})$] for Cyg OB2 #12 can be constructed.

4. Results and Discussions

4.1. Extinction Laws Toward V410 Anon9 and Cyg OB2 #12

The extinction results for V410 Anon9 and Cyg OB2 #12 are listed in Table 2. The fitting parameters and the 1σ

---

[8] We also adopted four free parameters ($\alpha_{\rm sil}$, $a_{\rm csil}$, $\alpha_{\rm gra}$, $a_{\rm cgra}$) for the fitting, and derived the similar results as those derived with two free parameters ($\alpha_{\rm sil}$, $\alpha_{\rm gra}$). However, by comparing the values of the Akaike information criterion for the model with four parameters and that with two parameters, we would prefer the latter model in this work for the better goodness of fitting.

Table 2
Derived Fitting Parameters and the Corresponding R_V, $E(B-V)$, A_V for V410 Anon9 and Cyg OB2 #12 Compared to the Previous Works

	α_{sil}	a_{csil} (μm)	α_{gra}	a_{cgra} (μm)	RSS[a]	R_V	$E(B-V)$ (mag)	A_V (mag)	References
V410 Anon9	$0.80^{+0.03}_{-0.03}$	$0.050^{+0.003}_{-0.003}$	$0.80^{+0.03}_{-0.03}$	$0.050^{+0.003}_{-0.003}$	1.05	4.26	2.40	10.24	EMCEE fitting code
	0.80	0.050	0.80	0.050	1.05	4.26	2.40	10.24	Levenberg–Marquardt method
	...	...	...	...	...	...		10.45	Strom & Strom (1994)
Cyg OB2 #12[b]	$4.65^{+0.03}_{-0.03}$	0.25	$3.60^{+0.03}_{-0.03}$	0.25	1.11	3.00	3.36	10.08	EMCEE fitting code
	4.70	0.25	3.60	0.25	1.11	3.00	3.36	10.08	Levenberg–Marquardt method
	...	...	...	...	...	3.00	3.34	10.02	Maryeva et al. (2016)
	...	...	...	...	...	3.04	3.36	10.20	Torres-Dodgen et al. (1991)

Notes.
[a] The residual sum of squares $= \sum [\log(f_{model}) - \log(f_{observed})]^2$.
[b] The same dust size distribution of silicate and graphite is adopted for V410 Anon9.

uncertainties are tabulated based on the 50%, 16%, and 84% values of the marginalized 1D posterior probability distribution functions generated from the EMCEE results. The fifth column shows the residual sum of squares (RSS) for both tracers calculated from the derived parameters. The sixth to eighth columns in Table 2 compare the corresponding R_V, $E(B-V)$ and A_V derived in this work and those in some former studies. R_V in this work is derived from the extinction curve

$$R_V = A_V / E(B-V) = 1/(A_B/A_V - 1), \qquad (4)$$

$E(B-V)$ is calculated by

$$E(B-V) = 2.5\log[(F_B^{int} F_V^{mod})/(F_V^{int} F_B^{mod})], \qquad (5)$$

and then

$$A_V = R_V \times E(B-V). \qquad (6)$$

The Levenberg–Marquardt method is also applied to fit the models to the observed data for comparison, and the same fitting parameters as those derived from the EMCEE fitting code can be derived. The best-fitting model SEDs for V410 Anon9 and Cyg OB2 #12 are compared with the observed photometry in Figure 3.

The A_V value derived for V410 Anon9 is about 1.9% smaller than that in Strom & Strom (1994), which was calculated from the observed magnitude and the intrinsic magnitude in the V band inferred based on the spectral type. The minor deviation may be due to the different effective wavelengths in the V band adopted in this work and Strom & Strom (1994). While the derived A_V value for Cyg OB2 #12 is similar to those in the former studies (e.g., Torres-Dodgen et al. 1991; Maryeva et al. 2016), and the tiny differences are attributed to different observed and intrinsic data adopted. The consistency of the extinction results derived in this work and the former studies shows the practicability and reliability of the improved pair method proposed in this work for calculating the extinction law toward individual sight line.

We present the derived extinction curves in Figure 4. The comparison of the two extinction curves will be discussed in the next subsection. Although all dust models for the diffuse ISM predict an extinction curve steeply declines with λ at $1\,\mu m < \lambda < 7\,\mu m$ and increases at $\lambda > 7\,\mu m$ because of the 9.7 μm silicate absorption feature (Mathis et al. 1977; Kim et al. 1994; Weingartner & Draine 2001), many recent observations suggest that the extinction law in the mid-IR band ($3\,\mu m < \lambda < 8\,\mu m$) appears to be almost universally flat or gray in various interstellar environments (Lutz et al. 1996; Lutz 1999; Indebetouw et al. 2005; Flaherty et al. 2007; Gao et al. 2009; Nishiyama et al. 2009; Fritz et al. 2011; Wang et al. 2013, 2015). Wang et al. (2015) modeled the extinction curve with μm-size grains together with a mixture of silicate and graphite grains of sizes ranging from a few angstroms to a few submicronmeter and found that the flat mid-IR extinction curve at ~3–8 μm provides a sensitive constraint on very large, μm-sized grains. The μm-sized grains bring gray extinction at optical wavelengths and the extinction curve from the far-UV to near-IR bands is not affected by the existence of the μm-sized grains. Although adding the μm-sized grains to the silicate-graphite dust model contributes to a better fit in the mid-IR bands, the model will become complex. In addition, the mid-IR observations cannot be obtained for all the tracers. As a result, the silicate-graphite dust model adopted in this work is more efficient and more universal to derive the extinction law from UV to near-IR. The extinction curves derived in this work presented in Figure 4 are reliable at $\lambda < 3\,\mu m$, while those at $\lambda > 3\,\mu m$ may suffer a large uncertainty.

The extinction curve toward Cyg OB2 #12 in this work is compared with that derived in Hensley & Draine (2020), showing consistency in the optical bands (~0.3–0.6 μm). The extinction curve in Hensley & Draine (2020) from the UV to near-IR bands is extracted from Fitzpatrick et al. (2019) and the minor difference between the extinction curve derived in this
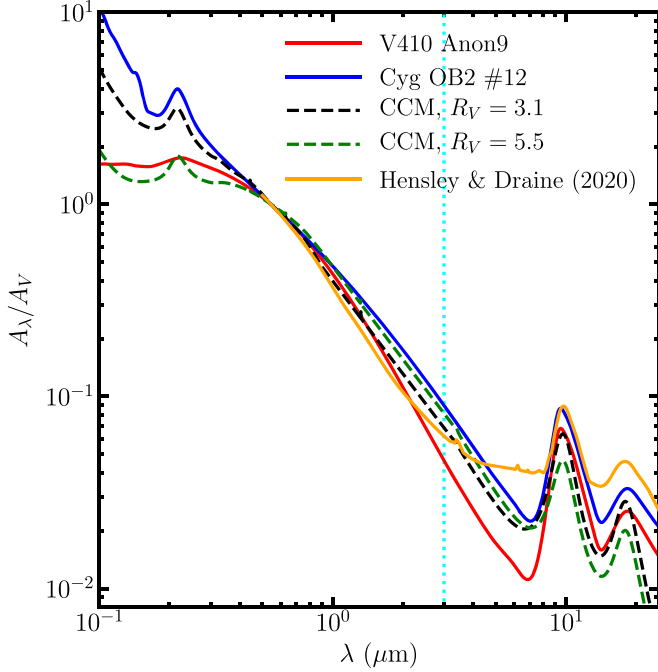
Figure 4. The extinction curves toward V410 Anon9 (red solid line) and Cyg OB2 # 12 (blue solid line) derived in this work compared with the CCM model. The orange line shows the extinction curve toward Cyg OB2 #12 from Hensley & Draine (2020). The cyan dotted line indicates $\lambda = 3\ \mu$m. The extinction curves derived in this work at $\lambda < 3\ \mu$m are reliable and effective (see Section 4.1 for the details).

Figure 5. The dust size distributions toward V410 Anon9 and Cyg OB2 # 12 derived in this work as well as the KMH dust size distributions of the silicate and graphite in the MW.

work and that from Hensley & Draine (2020) in the optical to near-IR bands is within the deviation of mean extinction curve given in Fitzpatrick et al. (2019).

4.2. Influence of Interstellar Environment on the Extinction Law

It is generally believed that the interstellar environment has a great influence on the extinction law. The size of grain in the dense region is larger, while smaller grain distributes in the diffuse region. V410 Anon9 is a typical extinction tracer in the dense region, and Cyg OB2 #12 is located in the diffuse region. The extinction curves derived for both tracers with the typical CCM extinction curves are shown in Figure 4, from which we can notice a remarkable distinction between the extinction laws toward both tracers, indicating different dust properties. By comparing the results of both tracers, we can explore how different interstellar environments impact on the properties of extinction. In addition, the application of the improved pair method proposed in this work to different interstellar environments can also be proved.

The extinction curve derived for V410 Anon9 is relatively flatter and shows a weaker 2175 Å bump feature indicating large dust size, which is in line with the properties of dust in the
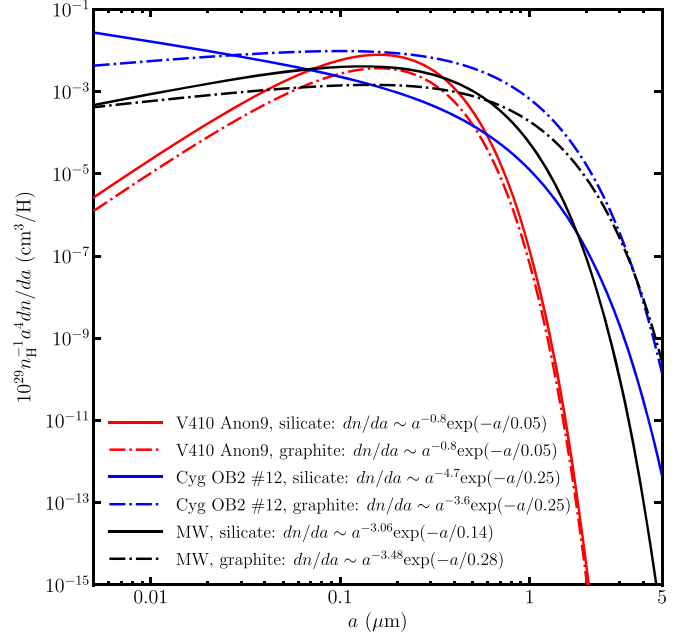
dense interstellar environment ($R_V \approx 5.5$). For Cyg OB2 #12, the extinction curve exhibits consistency to the mean extinction curve of the MW ($R_V \approx 3.1$), and the 2175 Å bump in the extinction curve is obvious. The significantly different absorption features at ~2175 Å in both extinction curves indicate that the dust size toward V410 Anon9 is larger than that toward Cyg OB2 #12.

In addition to the reliable extinction results, the parameters included in the dust model obtained from the improved pair method can also be used to analyze the dust properties quantitatively, which cannot be achieved by the mathematical extinction laws. We present the dust size distributions toward V410 Anon9 and Cyg OB2 #12 in Figure 5 as well as the KMH dust size distributions for silicate and graphite in the MW (Kim et al. 1994). Equation (8) in Nozawa (2016) is adopted to calculate the average dust size $\bar{a}$, and we derive that $\overline{a_{\rm sil}} = \overline{a_{\rm gra}} \approx 0.03\ \mu$m for V410 Anon9 and $\overline{a_{\rm sil}} \approx 0.006\ \mu$m, $\overline{a_{\rm gra}} \approx 0.007\ \mu$m for Cyg OB2 #12. Compared with $\overline{a_{\rm sil}} \approx 0.008\ \mu$m and $\overline{a_{\rm gra}} \approx 0.007\ \mu$m for the MW with the KMH distributions calculated from the same method, the average dust size of Cyg OB2 #12 is similar to that of the MW and is smaller than that of V410 Anon 9.

4.3. Influence of Stellar Parameters on the Extinction Law

The stellar parameters derived with the improved pair method for V410 Anon9 is that $\log(T_{\rm eff}) = 3.92^{+0.004}_{-0.005}$ and
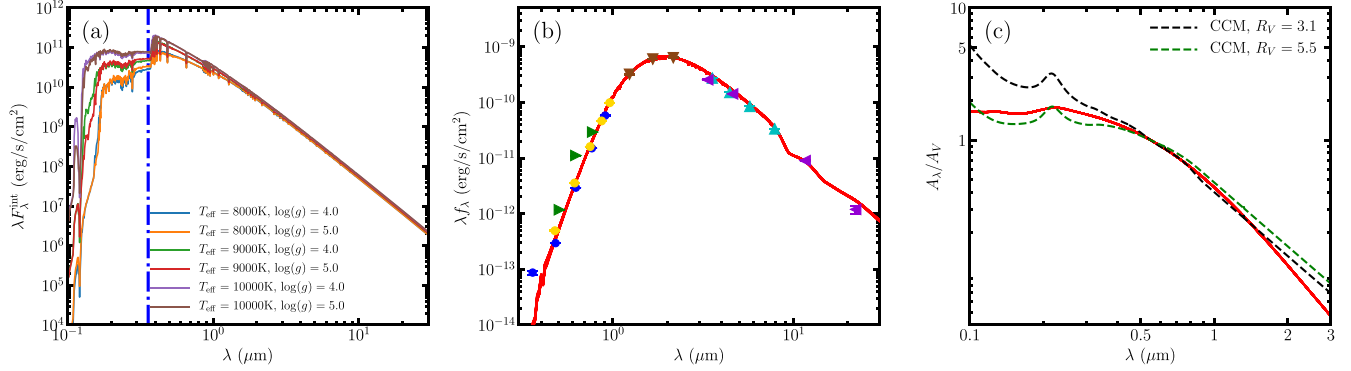
Figure 6. Tests for the sensitivity of the results to the stellar parameters. (a) Intrinsic spectra derived from the ATLAS9 stellar model atmosphere with different stellar parameters. The blue dashed-and-dotted line indicates the shortest effective wavelength of the observed photometry for V410 Anon9 ($\lambda = u_{\mathrm{eff}}$) in this work. (b) Best-fitting model SEDs derived from different possible stellar parameters adopted for V410 Anon9 compared with the observed photometry. (c) Extinction curves of V410 Anon9 derived with different possible stellar parameters.

$\log(g) = 4.24^{+0.172}_{-0.169}$. The derived value of $\log(g)$ is reasonable for the A-type main sequence star (Cox 2000), while the derived $\log(T_{\mathrm{eff}})$ is lower than that [$\log(T_{\mathrm{eff}}) \approx 3.95$] in Strom & Strom (1994). The intrinsic SED with the derived stellar parameters is presented in the upper panel of Figure 3 with a blue solid line compared to that with $\log(T_{\mathrm{eff}}) = 3.95$ and $\log(g) = 4.2$. For Cyg OB2 #12, we derived that $\log(T_{\mathrm{eff}}) = 4.14^{+0.056}_{-0.030}$ and $\log(g) = 1.60^{+0.125}_{-0.032}$, which corresponds to the estimated stellar parameters [$\log(T_{\mathrm{eff}}) = 4.14$ and $\log(g) = 1.7$] in Clark et al. (2012) and proves that the method proposed in this work can also be used to infer the stellar parameters.

As we know, different stellar parameters lead to different intrinsic SEDs, thus may lead to different derived extinction curves. As a result, it is necessary to find out the sensitivity of the extinction law to the stellar parameters. To show the influence of the stellar parameters on the intrinsic SEDs, we plot the intrinsic SEDs derived from the ATLAS9 stellar model atmosphere with different stellar parameters in Figure 6(a). The blue dashed-and-dotted line indicates the lower limit of effective wavelengths of the observed photometry that we adopt for V410 Anon9 in this work (u band). From Figure 6(a), we can find that $\log(g)$ has little effect on the intrinsic flux, while the intrinsic flux increases with the increase of T_{eff}, especially in UV and shorter bands.

As the spectral type of tracer V410 Anon9 is A2, we adopt some other possible values of $\log(g)$ and T_{eff} for the A-type main sequence star ($7300\,\mathrm{K} < T_{\mathrm{eff}} < 10{,}000\,\mathrm{K}$, $4.14 < \log(g) < 4.34$ according to Cox 2000) to test the sensitivity of the extinction law to the stellar parameters for V410 Anon9.

We list the results derived with the EMCEE fitting code for each pair of the stellar parameters in Table 3, which are the same as those derived with the Levenberg–Marquardt method, and compare the model SEDs with the observed data in Figure 6(b). The extinction curves derived with different stellar parameters are presented in Figure 6(c), while the derived

values of A_V ranging from 9.75 mag to 10.52 mag[9] are plotted in Figure 7. It is illustrated that the small variation of the stellar parameters in this work has little effect on the extinction curves and dust properties for V410 Anon9, because the intrinsic spectra at $\lambda > \lambda_u$ are not strongly influenced by the stellar parameters as presented in Figure 6. It is also suggested that even if the stellar parameters could not be obtained directly, we can still derive the extinction law and analyze the properties of the dust based on the spectral type of the tracer.

5. Summary of the Improved Method

An improved pair method is proposed in this work based on the traditional pair method. The improved method combines the intrinsic SEDs from the ATLAS9 stellar model atmosphere and the model extinction curves from the silicate-graphite dust model. Adopting a stellar model atmosphere to obtain intrinsic spectra is to eliminate the impact of the limited standard stars (Fitzpatrick & Massa 2005). While extinction curves from the dust model can be applied to various interstellar environments and help to analyze the dust properties. The pre-construction of the template library for the model SEDs greatly reduces the time required for the calculation. V410 Anon9 located in the dense region of the MW and Cyg OB2 #12 located in the diffuse region of the MW are chosen as the extinction tracers, and the derived results are consistent with their interstellar environments and the previous studies. It is proved that the improved pair method proposed in this work is reliable and efficient to calculate the dust extinction law from UV to near-IR bands toward various interstellar environments. In addition

---

9 The color changes mimic the effect of extinction, so there are degeneracies between the effective temperature and the extinction values. However, thanks to the wide wavelength coverage of the observations, the results derived by the method proposed in this work are not affected by the degeneracy between the effective temperature and the extinction values according to the parameter sensitivity tests in Wang et al. (2022a).
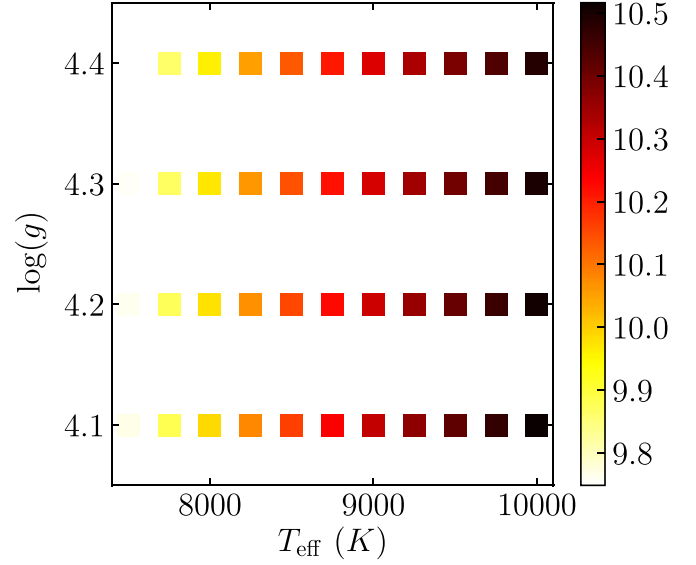
Table 3
The Derived Fitting Parameters, (α, a_c) and the Corresponding A_V for V410
Anon9 with Different Possible Stellar Parameters Adopted[a]

$T_{\rm eff}$ (K)	$\log(g)$	α	a_c (μm)	A_V (mag)
8995	4.2	$0.8^{+0.03}_{-0.03}$	$0.05^{+0.003}_{-0.003}$	10.29
7500	4.1	$0.8^{+0.03}_{-0.03}$	$0.05^{+0.003}_{-0.003}$	9.77
	4.2	$0.8^{+0.03}_{-0.03}$	$0.05^{+0.003}_{-0.003}$	9.76
	4.3	$0.8^{+0.03}_{-0.03}$	$0.05^{+0.003}_{-0.003}$	9.75
	4.4	$0.8^{+0.03}_{-0.03}$	$0.05^{+0.003}_{-0.003}$	9.75
8000	4.1	$0.8^{+0.03}_{-0.03}$	$0.05^{+0.003}_{-0.003}$	9.99
	4.2	$0.8^{+0.03}_{-0.03}$	$0.05^{+0.003}_{-0.003}$	9.98
	4.3	$0.8^{+0.03}_{-0.03}$	$0.05^{+0.003}_{-0.003}$	9.97
	4.4	$0.8^{+0.03}_{-0.03}$	$0.05^{+0.003}_{-0.003}$	9.96
8500	4.1	$0.8^{+0.03}_{-0.03}$	$0.05^{+0.003}_{-0.003}$	10.16
	4.2	$0.8^{+0.03}_{-0.03}$	$0.05^{+0.003}_{-0.003}$	10.15
	4.3	$0.8^{+0.03}_{-0.03}$	$0.05^{+0.004}_{-0.003}$	10.14
	4.4	$0.8^{+0.03}_{-0.03}$	$0.05^{+0.003}_{-0.003}$	10.13
9000	4.1	$0.8^{+0.03}_{-0.03}$	$0.05^{+0.003}_{-0.003}$	10.3
	4.2	$0.8^{+0.03}_{-0.03}$	$0.05^{+0.003}_{-0.003}$	10.29
	4.3	$0.8^{+0.03}_{-0.03}$	$0.05^{+0.003}_{-0.003}$	10.28
	4.4	$0.8^{+0.03}_{-0.03}$	$0.05^{+0.003}_{-0.003}$	10.27
9500	4.1	$0.8^{+0.03}_{-0.03}$	$0.05^{+0.004}_{-0.003}$	10.42
	4.2	$0.8^{+0.03}_{-0.03}$	$0.05^{+0.003}_{-0.003}$	10.41
	4.3	$0.8^{+0.03}_{-0.03}$	$0.05^{+0.003}_{-0.003}$	10.4
	4.4	$0.8^{+0.04}_{-0.03}$	$0.05^{+0.003}_{-0.003}$	10.39
10000	4.1	$0.8^{+0.03}_{-0.03}$	$0.05^{+0.003}_{-0.003}$	10.52
	4.2	$0.8^{+0.03}_{-0.03}$	$0.05^{+0.003}_{-0.003}$	10.51
	4.3	$0.8^{+0.03}_{-0.03}$	$0.05^{+0.003}_{-0.003}$	10.5
	4.4	$0.8^{+0.04}_{-0.03}$	$0.05^{+0.003}_{-0.003}$	10.49

Note.
[a] The first line is the results for V410 Anon9 with $T_{\rm eff}$ from Strom & Strom (1994) and $\log(g)$ based on the spectral type.

Figure 7. The values of A_V derived for A-type main sequence stars with different stellar parameters.

to the reliable extinction results, the dust properties can be analyzed and the stellar parameters can be inferred with the improved pair method at the same time. Furthermore, the extinction law beyond the wavelengths of observed data can also be predicted based on the dust model.

However, as mentioned in Section 4.1, the improved pair method may not be applied in the mid-IR band, because the extinction curves derived from the silicate-graphite model in the mid-IR band ($\sim$3–8 μm) are not as flat as the extinction law calculated from the recent observations. Although the μm-sized grain can contribute to modeling the flat mid-IR extinction curve (Wang et al. 2015), it will increase the complexity of the model and thus reduce the universality of the improved method. As a result, the improved pair method proposed in this work can be used to derive the extinction curve from UV to near-IR bands at present. In addition, the reliability of the improved pair method depends on the wavelength coverage of the observed data. Lacking UV or near-IR data may lead to

unreliable results (Wang et al. 2022a). To obtain more appropriate extinction curves with the improved pair method, observed data that cover the wavelength from UV to near-IR are needed.

The improved pair method proposed in this work can be applied to large-scale samples in the MW and external galaxies. Despite the unknown stellar parameters, dozens of extinction curves toward individual sight lines have been derived in M31 (Wang et al. 2022a), M33 (Wang et al. 2022b), and other external galaxies (Wang et al. 2022b) based on the spectral types of the extinction tracers. In addition, the coming 2 m aperture Survey Space Telescope (also known as the China Space Station Telescope, CSST, Zhan 2021) will image the sky and will provide us with abundant data in the UV to IR bands with high resolution. We can combine the improved pair method with the multi-band photometry from the CSST to get a more comprehensive understanding of the dust extinction law and dust properties in the MW and external galaxies.

Acknowledgments

Galaxies Survey on Dust and Extinction Project CMS-CSST-2021-A09.

ORCID iDs

Yuxi Wang ⦿ https://orcid.org/0000-0003-3860-5286
Jian Gao ⦿ https://orcid.org/0000-0003-4195-0195
Yi Ren ⦿ https://orcid.org/0000-0003-1218-8699
Jun Li ⦿ https://orcid.org/0000-0001-9328-4302

References

Abrahamyan, H. V., Mickaelian, A. M., & Knyazyan, A. V. 2015, A&C, 10, 99
Aguado, D. S., Ahumada, R., Almeida, A., et al. 2019, ApJS, 240, 23
Amanullah, R., Johansson, J., Goobar, A., et al. 2015, MNRAS, 453, 3300
Asplund, M., Grevesse, N., Sauval, A. J., & Scott, P. 2009, ARA&A, 47, 481
Bless, R. C., & Savage, B. D. 1970, Observations of Interstellar Extinction in the Ultraviolet with the OAO Satellite, in IAU Symp. 36, ed. R. Muller, L. Houziaux, & H. E. Butler (Dordrecht: D. Reidel), 28
Caballero-Nieves, S. M., Nelan, E. P., Gies, D. R., et al. 2014, AJ, 147, 40
Cardelli, J. A., Clayton, G. C., & Mathis, J. S. 1989, ApJ, 345, 245
Chambers, K. C., Magnier, E. A., Metcalfe, N., et al. 2016, arXiv:1612.05560
Chentsov, E. L., Klochkova, V. G., Panchuk, V. E., Yushkin, M. V., & Nasonov, D. S. 2013, ARep, 57, 527
Churchwell, E., Babler, B. L., Meade, M. R., et al. 2009, PASP, 121, 213
Clark, J. S., Najarro, F., Negueruela, I., et al. 2012, A&A, 541, A145
Clayton, G. C., Gordon, K. D., Bianchi, L. C., et al. 2015, ApJ, 815, 14
Cox, A. N. 2000, IrAJ, 27, 234
Cox, R. T. 1946, AmJPh, 14, 1
Cui, X.-Q., Zhao, Y.-H., Chu, Y.-Q., et al. 2012, RAA, 12, 1197
Cutri, R. M., Skrutskie, M. F., van Dyk, S., et al. 2003, yCat, II/246
Cutri, R. M., Wright, E. L., Conrow, T., et al. 2013, Explanatory Supplement to the AllWISE Data Release Products, 1 WISE
D'Orazi, V., Biazzo, K., & Randich, S. 2011, A&A, 526, A103
Draine, B. T. 2003, ARA&A, 41, 241
Draine, B. T. 2011, in Physics of the Interstellar and Intergalactic Medium, ed. D. N. Spergel (Princeton, NJ: Princeton Univ. Press)
Draine, B. T., & Lee, H. M. 1984, ApJ, 285, 89
Egan, M. P., Price, S. D., Kraemer, K. E., et al. 2003, yCat
Fitzpatrick, E. L. 1999, PASP, 111, 63
Fitzpatrick, E. L. 2004, in ASP Conf. Ser. 309, Interstellar Extinction in the Milky Way Galaxy, Astrophysics of Dust, ed. A. N. Witt, G. C. Clayton, & B. T. Draine (San Francisco, CA: ASP), 33
Fitzpatrick, E. L., & Massa, D. 1990, ApJS, 72, 163
Fitzpatrick, E. L., & Massa, D. 2005, AJ, 130, 1127
Fitzpatrick, E. L., Massa, D., Gordon, K. D., Bohlin, R., & Clayton, G. C. 2019, ApJ, 886, 108
Flaherty, K. M., Pipher, J. L., Megeath, S. T., et al. 2007, ApJ, 663, 1069
Foreman-Mackey, D., Hogg, D. W., Lang, D., & Goodman, J. 2013, PASP, 125, 306

Fritz, T. K., Gillessen, S., Dodds-Eden, K., et al. 2011, ApJ, 737, 73
Gaia Collaboration 2018, yCat, I/345
Gao, J., Jiang, B. W., & Li, A. 2009, ApJ, 707, 89
Gao, J., Jiang, B. W., Li, A., Li, J., & Wang, X. 2015, ApJL, 807, L26
Gao, W., Zhao, R., Gao, J., Jiang, B., & Li, J. 2020, P&SS, 183, 104627
Goodman, J., & Weare, J. 2010, Communications in Applied Mathematics and Computational Science, 5, 65
Gordon, K. D., Clayton, G. C., Misselt, K. A., Land olt, A. U., & Wolff, M. J. 2003, ApJ, 594, 279
Greenberg, J. M. 1978, in Cosmic Dust, ed. J. A. M. McDonnell (Chichester: Wiley), 187
Guarcello, M. G., Wright, N. J., Drake, J. J., et al. 2012, ApJS, 202, 19
Hanson, M. M. 2003, ApJ, 597, 957
Hensley, B. S., & Draine, B. T. 2020, ApJ, 895, 38
Indebetouw, R., Mathis, J. S., Babler, B. L., et al. 2005, ApJ, 619, 931
Ishihara, D., Onaka, T., Kataza, H., et al. 2010, A&A, 514, A1
Kim, S.-H., Martin, P. G., & Hendry, P. D. 1994, ApJ, 422, 164
Kiminki, D. C., Kobulnicky, H. A., Kinemuchi, K., et al. 2007, ApJ, 664, 1102
Kurucz, R. L. 1970, SAOSR
Li, A., & Draine, B. T. 2001, ApJ, 554, 778
Li, A., & Greenberg, J. M. 1997, A&A, 323, 566
Li, J., Gao, J., Jiang, B., & Lin, Z. 2022, MNRAS, 511, 2021
Lutz, D. 1999, in The Universe as Seen by ISO, ed. P. Cox & M. Kessler (Pairs: ESA-SP), 623
Lutz, D., Feuchtgruber, H., Genzel, R., et al. 1996, A&A, 315, L269
Maryeva, O. V., Chentsov, E. L., Goranskij, V. P., et al. 2016, MNRAS, 458, 491
Mathis, J. S., Rumpl, W., & Nordsieck, K. H. 1977, ApJ, 217, 425
Mathis, J. S., & Whiffen, G. 1989, ApJ, 341, 808
Nishiyama, S., Tamura, M., Hatano, H., et al. 2009, ApJ, 696, 1407
Nozawa, T. 2016, P&SS, 133, 36
Ofek, E. O. 2008, PASP, 120, 1128
Oskinova, L. M., Huenemoerder, D. P., Hamann, W. R., et al. 2017, ApJ, 845, 39
Page, M. J., Brindle, C., Talavera, A., et al. 2019, yCat, II/356
Sharpless, S. 1957, PASP, 69, 239
Shenoy, S. S., Whittet, D. C. B., Ives, J. A., & Watson, D. M. 2008, ApJS, 176, 457
Strom, K. M., & Strom, S. E. 1994, ApJ, 424, 237
Torres-Dodgen, A. V., Tapia, M., & Carroll, M. 1991, MNRAS, 249, 1
Wang, S., Gao, J., Jiang, B. W., Li, A., & Chen, Y. 2013, ApJ, 773, 30
Wang, Y., Gao, J., & Ren, Y. 2022a, ApJS, 259, 12
Wang, Y., Gao, J., Ren, Y., & Chen, B. 2022b, ApJS, 260, 41
Wang, S., Li, A., & Jiang, B. W. 2015, ApJ, 811, 38
Weingartner, J. C., & Draine, B. T. 2001, ApJ, 548, 296
Whittet, D. C. B. 2015, ApJ, 811, 110
Wright, N. J., Drake, J. J., Drew, J. E., & Vink, J. S. 2010, ApJ, 713, 871
Wright, N. J., Drew, J. E., & Mohr-Smith, M. 2015, MNRAS, 449, 741
Zhan, H. 2021, ChSBu
Zhao, G., Zhao, Y.-H., Chu, Y.-Q., Jing, Y.-P., & Deng, L.-C. 2012, RAA, 12, 723
Zubko, V., Dwek, E., & Arendt, R. G. 2004, ApJS, 152, 211